PAPER

CrossMark
← click for updates

Supported bimetallic nano-alloys as highly active catalysts for the one-pot tandem synthesis of imines and secondary amines from nitrobenzene and alcohols†

Meenakshisundaram Sankar,*[ab] Qian He,[c] Simon Dawson,[b] Ewa Nowicka,[b] Li Lu,[c] Pieter C. A. Bruijnincx,[a] Andrew M. Beale,[de] Christopher J. Kiely[c] and Bert M. Weckhuysen*[a]

The synthesis and functionalization of imines and amines are key steps in the preparation of many fine chemicals and for pharmaceuticals in particular. Traditionally, metal complexes are used as homogeneous catalysts for these organic transformations. Here we report gold–palladium and ruthenium–palladium nano-alloys supported on TiO_2 acting as highly efficient heterogeneous catalysts for the one-pot synthesis of the imine *N*-benzylideneaniline and the secondary amine *N*-benzylaniline directly from the easily available and stable nitrobenzene and benzyl alcohol precursors using a hydrogen auto-transfer strategy. These reactions were carried out without any added external hydrogen, sacrificial hydrogen donor or a homogeneous base. The bimetallic catalysts were prepared by the recently developed modified impregnation strategy, giving efficient control of size and nano-alloy composition. Both bimetallic catalysts were found to be far more active than their monometallic analogues due to a synergistic effect. Based on the turnover numbers the catalytic activities follow the order Ru < Pd < Au ≪ Au–Pd < Ru–Pd. Aberration corrected scanning transmission electron microscopy (AC-STEM) and X-ray absorption spectroscopy (XAFS) studies of these catalysts revealed that the reason for the observed synergistic effect is the electronic modification of the metal sites in the case of the Au–Pd system and a size stabilisation effect in the case of the Ru–Pd catalyst.

[a] *Inorganic Chemistry and Catalysis, Debye Institute for Nanomaterials Science, Utrecht University, Universiteitsweg 99, 3584 CG Utrecht, The Netherlands. E-mail: B.M.Weckhuysen@uu.nl*
[b] *Cardiff Catalysis Institute, School of Chemistry, Cardiff University, Cardiff CF10 3AT, UK. E-mail: Sankar@cardiff.ac.uk; Tel: +44 (0)29 2087 5748*
[c] *Department of Material Science and Engineering, Lehigh University, 5 East Packer Avenue, Bethlehem, PA 18015-3195, USA*
[d] *Research Complex at Harwell, Rutherford Appleton Laboratory, Oxfordshire, OX11 0FA, UK*
[e] *Department of Chemistry, University College London, 20 Gordon Street, London WC1H 0AJ, UK*
† Electronic supplementary information (ESI) available. See DOI: 10.1039/c6cy00425c

Introduction

Supported bimetallic nano-alloys exhibit substantially different, often enhanced, properties compared to their monometallic analogues, which makes them very attractive for various technical applications, especially as catalysts.[1] Precise control of their structural parameters, such as (a) size-dependent compositional variation, (b) morphology and (c) monodispersity of particle size, is crucial to fully harness the catalytic power of these bimetallic nano-alloys.[2,3] Conventionally, supported bimetallic nano-alloys are prepared by a wet-impregnation (C_{Im}) method using aqueous solutions containing both metal precursors and the support. Catalysts prepared by this route normally contain metal particles ranging from sub-nm metal clusters to a few micron-sized particles.[3] To overcome this problem of the broad size distribution, size-controlled nano-alloys have been prepared in aqueous solutions in the presence of stabilizer ligands, such as polyvinyl alcohol (PVA) or poly(vinylpyrrolidone) (PVP).[4] These particles are then immobilized onto a solid oxide support (sol-immobilization (S_{Im}) method) to form catalysts with almost all the metal particles existing within the 2–10 nm range.[5] However, supported nano-alloys prepared by the S_{Im} method still tend to exhibit a size-dependent composition variation.[6,7]

Recently, Sankar *et al.* reported an excess anion modification of the C_{Im} method (the modified impregnation (M_{Im}) method) for the synthesis of supported gold–palladium nano-alloys, which affords a more precise control over size, composition and morphology.[8] By adding excess hydrochloric acid to the Au and Pd precursors in the wet-impregnation stage,

This journal is © The Royal Society of Chemistry 2016

Catal. Sci. Technol., 2016, **6**, 5473–5482 | 5473

and subsequent direct gas-phase reduction, Au–Pd alloy particle size can be controlled to be within the 1–6 nm range with no size significant dependent composition variation of Au and Pd. Occasionally, some micron-scale Au-rich particles were found in some of the M_{Im} derived Au–Pd catalysts. Such micron-sized particles could be completely eliminated, though, by increasing the hydrochloric acid concentration during the preparation stage. However, the latter catalyst, i.e., without any micron-sized gold-rich particles, was found to be unstable for catalytic applications, whereas the former catalyst with occasional micron-scale particles was found to be stable for catalytic re-use.[8] The stable bimetallic catalysts showed significant improvements in the catalytic activities for the direct synthesis of hydrogen peroxide and the aerobic benzyl alcohol oxidation reactions.[10] Very recently, we also reported the synthesis of supported Ru–Pd catalysts, using the same M_{Im} route; no micron-scale particles were detected for these catalysts, suggesting all of the metal precursors are converted into alloyed nanoparticles with controlled size and composition. These supported bimetallic Ru–Pd nano-alloy catalysts were exceptionally active, selective and stable in the hydrogenation of biomass derived levulinic acid to γ-valerolactone.[9]

Dehydrogenation reactions are often carried out in the presence of stoichiometric amounts or a large excess of oxygen, peroxides, iodates, metal oxides or sacrificial hydrogen acceptors to circumvent the thermodynamic restrictions associated with such dehydrogenations.[10] In all these processes, the liberated hydrogen is "*wasted*" and ends up in hydrogenated by-products (e.g., H_2O). An example of this kind of reaction is the oxidative dehydrogenation of benzyl alcohol to benzaldehyde, where oxygen is used as the sacrificial hydrogen acceptor to form water.[11] From an atom-economic perspective, the expensive hydrogen produced by the dehydrogenation reaction should be more effectively used (in situ), for instance in a coupled hydrogenation reaction. Here, we demonstrate such an efficient use of the hydrogen liberated in the dehydrogenation of benzyl alcohol (1), by using nitrobenzene (3) as the hydrogen-acceptor rather than O_2 thus reducing nitrobenzene effectively to aniline (4). The products of these reactions, i.e., benzaldehyde (2) and aniline, readily couple to form N-benzylideneaniline (5). When 1 is used in excess, 5 is further hydrogenated to N-benzylaniline (6) (Fig. 1). Furthermore, the rate of the overall reaction increases with the increase in the amount of alcohol. This sequence of reactions has been previously reported and are known as acceptor-less dehydrogenation reactions, hydrogen auto-transfer reactions or as a borrowing hydrogen strategy.[10,12,13] Such reactions have proven extremely valuable for the synthesis of an assortment of useful compounds, including amines and amides, without stoichiometric reagents and harmful by-products. However in order to compete with the economically more advantageous conventional strategies using molecular H_2, the catalysts for these hydrogen-auto transfer processes have to be exceptionally active and selec-

Step-1: Synthesis of aniline

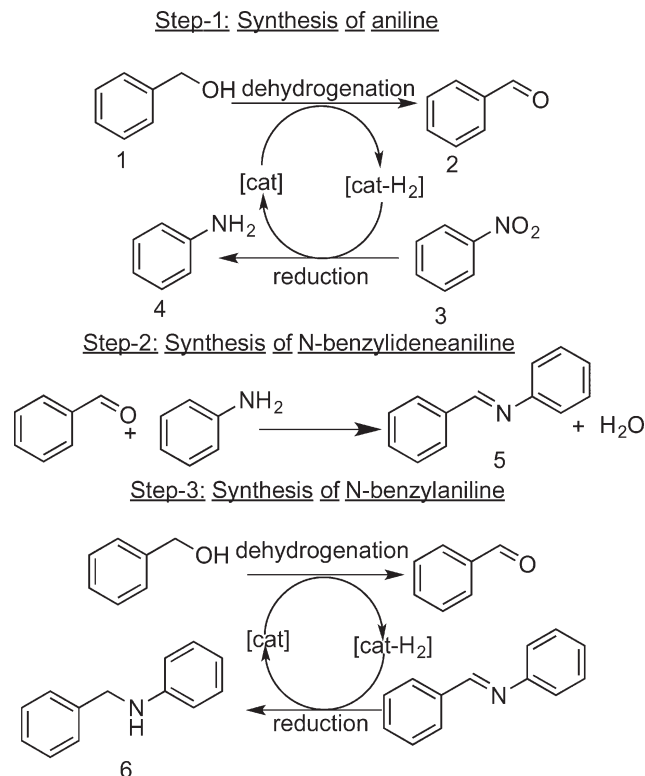Step-2: Synthesis of N-benzylideneaniline

Step-3: Synthesis of N-benzylaniline

Fig. 1 Sequence of reactions involved in the one-pot tandem synthesis of N-benzylideneaniline (5) and N-benzylaniline (6) from nitrobenzene (3) and benzyl alcohol (1).

tive. Various heterogeneous catalysts have been reported for the N-alkylation of aniline using benzyl alcohol using this strategy.[14,15] However, only a few catalytic systems have been reported for the direct synthesis of imines and N-alkylamines from nitroarenes and alcohols using this hydrogen auto transfer strategy. Most of these use homogeneous Ru, Ir or Pd-based metal complexes.[15–18] To the best of our knowledge, only a few research groups have used heterogeneous catalysts for this transformation process, and most of these systems require a homogeneous base for this direct transformation of nitrobenzene and benzyl alcohol to the corresponding benzyl imines and amines.[19,20] Two groups have reported the use of supported monometallic gold nanoparticles for this one-pot synthesis.[21,22]

Here, we show that supported gold–palladium and ruthenium–palladium nano-alloys are efficient catalysts for this hydrogen auto-transfer reaction, greatly surpassing the catalytic activities of their supported monometallic counterparts when prepared and tested under identical reaction conditions. Using abberation corrected scanning transmission electron microscopy (AC-STEM) and X-ray absorption spectroscopy (XAFS) characterisation data, we rationalise the observed catalytic behaviour of these supported gold–palladium and ruthenium–palladium nano-alloy catalysts.

Experimental

Synthesis of catalysts

Catalyst synthesis by the modified impregnation (M_{Im}) method. All the monometallic and bimetallic catalysts were prepared *via* the recently reported synthesis procedure.[9] The supports (TiO₂, (P25, Evonik), C (DARCO®, activated charcoal, Sigma Aldrich) and MgO (Sigma Aldrich)) were used without any further modification. In a typical catalyst synthesis procedure, $HAuCl_4 \cdot xH_2O$ (>99.9% pure, Sigma Aldrich) was used as the gold precursor and was dissolved in deionized water to form a solution with a gold concentration of 9.34 mg mL^{-1}. $RuCl_3$ (99.9%, Acros Chemicals) was used as the ruthenium precursor and was dissolved in deionized water to form an aqueous solution with a ruthenium concentration of 5.28 mg mL^{-1}. The $PdCl_2$ salt (<99%, Sigma Aldrich) was dissolved in 0.1 M HCl (concentrated HCl was diluted using the requisite amount of deionized water) with vigorous stirring and gentle warming with a resultant palladium concentration of 3.02 mg mL^{-1}. This solution was slowly cooled and used as the palladium precursor. In a typical catalyst synthesis, the requisite amount of the precursor solution(s) was charged into a clean 50 mL round bottomed flask fitted with a magnetic stirrer and then the solution was made up to 25 mL with deionized water. This flask was submerged in a temperature-controlled oil bath and the mixture was then agitated at 298 K using a hot plate stirrer (1200 rpm). After 15 min of stirring, the required amount of support was gradually added with constant stirring at 298 K over a period of 30 min. After completion of the support addition, the slurry was stirred vigorously at 298 K for about 30 min and then the oil bath temperature was raised to 333 K, stirred for 1 h and then finally heated to 358 K. The slurry was stirred at this temperature overnight until all the water had evaporated. The solid powder, denoted as the "dried sample", was ground thoroughly with a mortar and pestle and approximately 350 mg of this material was then reduced in a furnace at 723 K (approx. 2 K min^{-1} ramp rate) under a flow of 5% H₂/He (total flow: 420 mL min^{-1}) for 4 h. Finally, the furnace was cooled rapidly to room temperature and the catalyst sample was used without any further modification. All catalysts were prepared with a 1 wt% metal concentration on a 1 g production scale and in the case of bimetallic catalysts, the metal amounts were chosen to be equimolar. All the catalysts prepared by this method are labelled (M_{Im}) and were used in the hydrogen auto-transfer reaction without any further modification.

Catalyst synthesis by the sol immobilization (S_{Im}) method. The supported bimetallic gold–palladium catalysts were prepared by adapting a procedure reported elsewhere.[23] The supports (TiO₂, (P25, Evonik), C (DARCO®, activated charcoal, Sigma Aldrich) and MgO (Sigma Aldrich)) were used without any further modification. In a typical synthesis of 1% AuPd/TiO₂ (S_{Im}), the requisite amount of the precursor solutions were added to 800 mL of deionised water and stirred vigorously at 298 K. In parallel, an aqueous solution of 1 wt% polyvinyl alcohol (PVA, Sigma Aldrich, M.mt. = 10 000, 80% hydrolysed)

and an aqueous solution of 0.1 M NaBH₄ were also prepared. To an aqueous solution of the precursors, the requisite amount of the PVA solution was added (PVA/Au + Pd (wt/wt) = 1.3) and stirred for 30 min. Following this, the requisite amount of the freshly prepared aqueous solution of NaBH₄ (NaBH₄/Au + Pd (mol/mol) = 5) was added all at once to the stirring solution to instigate bimetallic sol formation. The solution was then stirred for a further 30 min to complete the sol formation. Subsequently, the required amount of support (TiO₂, Evonik-Degussa P25) was added. After several minutes of stirring, a drop of concentrated H₂SO₄ was added under vigorous stirring. The total target metal loading was calculated to be 1 wt% with equimolar metal amounts for the bimetallic catalysts. After 2 h of stirring, the slurry was filtered and the solid catalyst was washed thoroughly with 2 L of distilled water until the mother liquor became neutral. The filtered solid was then dried at 393 K overnight under static air and was used as a catalyst without any further modification. All the catalysts prepared by this method are labelled (S_{Im}).

Hydrogen auto-transfer reactions. The hydrogen auto-transfer reactions were carried out in a 50 mL stainless steel high pressure autoclave reactor (Parr Instruments) fitted with an overhead stirrer (1200 rpm). In a typical reaction, the reactor was charged with the requisite amount of all components (*i.e.*, alcohol, nitrobenzene, solvent and catalyst), and purged three times with He before being sealed with 20 bar of He. The pressure inside the reactor was monitored using both a manual pressure gauge and a digital pressure transducer. The reactor content was stirred at 1200 rpm under heated conditions. The reaction was assumed to commence when the reaction mixture temperature was 5 K lower than the set temperature. A reusability study and hot filtration study were performed in a 50 mL Radley's glass reactor at 413 K and at a pressure of 1 bar of He. At the end of the reaction, the reactor was cooled to 283 K using an ice bath after which the pressure was released; the reaction mixture was then removed and filtered. Finally, 1 g of the reaction mixture (along with 0.1 g of *n*-dodecane (external standard)) was injected into the GC (Shimadu GC-2010A gas chromatograph equipped with a WCOT fused silica CP-WAX 57-CB column and FID detector and a Varian 3800 GC fitted with a CP-WAX-52CB column and FID detector). Quantitative analyses were done using standard calibration mixtures of authentic samples of the reactants and products. The total turnover number (Total TON) was calculated using the formula

$$\text{Total TON} = [\text{mol}_{(3)} \text{ converted/mol}_{\text{total metal in the catalyst}}].$$

The amine turnover number (Amine TON) was calculated using the formula

$$\text{Amine TON} = [\text{mol}_{(6)} \text{ formed/mol}_{\text{total metal in the catalyst}}].$$

Product selectivity is defined as the fraction of the identified products. The products from benzyl alcohol dehydrogenation and disproportionation (benzaldehyde and toluene) have not been quantified.

This journal is © The Royal Society of Chemistry 2016

*Catal. Sci. Technol.*, 2016, **6**, 5473–5482 | **5475**

Catalyst characterisation. Samples for examination by scanning transmission electron microscopy (STEM) were prepared by dispersing the dry catalyst powder onto a holey carbon film supported by a 300 mesh copper TEM grid. STEM high angle annular dark field (HAADF) images of the metallic particles were obtained using an aberration corrected JEM ARM-200CF STEM operating at 200 kV. X-ray energy dispersive (XEDS) spectra were acquired from individual nanoparticles larger than 1 nm in size by rastering the beam over the entire particle, while using a JEOL Centurio 0.9 sr silicon drift detector. The sample powders were also dispersed onto an Al-stub and examined in a Hitachi 4300LV scanning electron microscope (SEM) equipped with an EDAX energy dispersive X-ray spectrometer to determine if there were any μm scale metal particles present. X-ray absorption fine structure (XAFS) spectroscopy measurements were performed on station BM26A and BM23 at the ESRF.[24] The measurements were carried out in transmission mode using a Si(111) monochromator at the Au L_3 edge, Pd K-edge and Ru K-edge with the respective monometallic foils used as reference materials. All data were subjected to background correction using Athena (*i.e.* IFFEFFIT software package) followed by either single or dual shell EXAFS fitting analyses performed using the DL-EXCURV program.[25]

Results and discussion

All the monometallic and bimetallic catalysts (1% Au/TiO$_2$ (M$_{Im}$), 1% Ru/TiO$_2$ (M$_{Im}$), 1% Pd/TiO$_2$(M$_{Im}$), 1% Au–Pd/TiO$_2$ (M$_{Im}$) and 1% Ru–Pd/TiO$_2$ (M$_{Im}$)), prepared by the M$_{Im}$ method, were tested for the one-pot tandem synthesis of **5** and **6** from **3** and excess of **1** at 433 K under an inert atmosphere. From the results (Fig. 2) it is evident that the bimetallic catalysts greatly out perform their monometallic counterparts. The total turnover number (TON$_{tot}$), based on molar conversion of **3**, and the amine turnover number (TON$_{amine}$), based on the yield of **6**, were used as a measure of catalytic activity. After 3 h, the TON$_{tot}$ values of these monometallic catalysts follow the order 1% Au/TiO$_2$ (340) > 1% Pd/TiO$_2$ (102) > 1% Ru/TiO$_2$ (53) and this catalytic activity trend matches that previously reported for this reaction.[21,22] The TON$_{amine}$ values for these monometallic 1% Au/TiO$_2$, 1% Pd/TiO$_2$, and 1% Ru/TiO$_2$ catalysts are 2, 1 and 1, respectively. Notably, the bimetallic catalysts showed a dramatic increase in the TON$_{tot}$ values with 475 and 787 for the 1% RuPd/TiO$_2$ and 1% AuPd/TiO$_2$ catalysts respectively. Based on the TON$_{amine}$ values the reactivity order follows 1% Ru–Pd/TiO$_2$ (174) > 1% Au–Pd/TiO$_2$ (93) ≫ monometallic catalysts. A time-on-line study for the most active supported ruthenium palladium bimetallic catalyst (1% Ru–Pd/TiO$_2$) at 433 K, clearly indicates the reduction of **3** and the formation of **5** to be kinetically more favourable than the reduction of **5** to **6** (Fig. 3). Notably, the selectivity to **5** is always maintained high (>90%) until the conversion level reaches 99%. Throughout this reaction, the selectivity for aniline (**4**) remained less than 1%, which indicates that the coupling of **4** and **2** is very fast. The corresponding time-on-line evolution of the TONs is presented in the ESI† (Fig. S1). A few examples
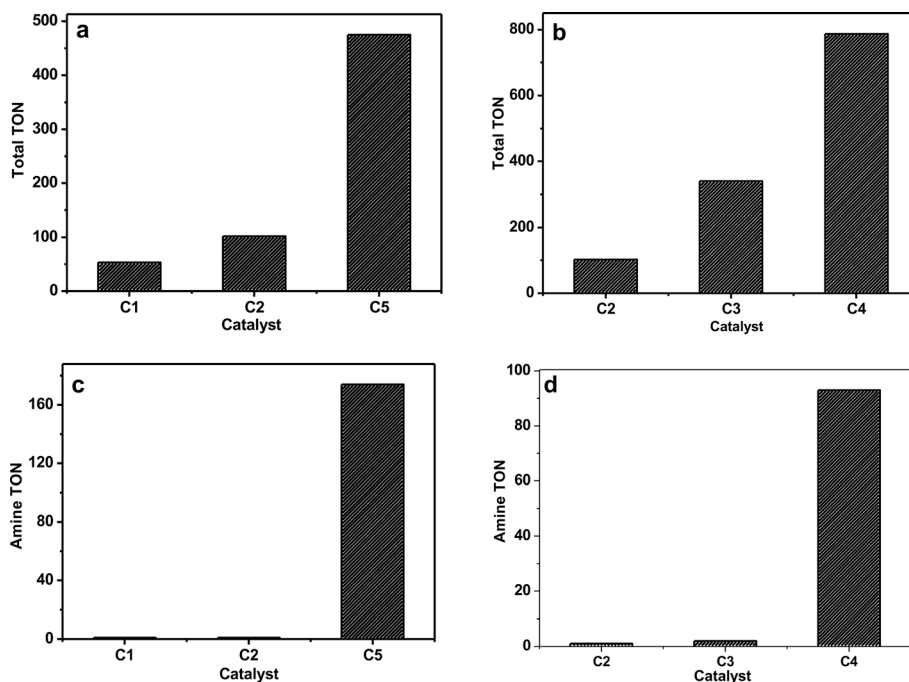
Fig. 2 Comparison of TONs of monometallic and bimetallic catalysts for the tandem synthesis of 5 and 6. (a): Ru and Pd for total TON; (b): Au and Pd for total TON; (c): Ru and Pd for amine TON and (d): Au and Pd for amine TON; key; C1: 1% Ru/TiO$_2$; C2: 1% Pd/TiO$_2$; C3: 1% Au/TiO$_2$; C4: 1% Au–Pd/TiO$_2$; C5: 1% Ru–Pd/TiO$_2$. Reaction conditions: catalyst: 0.1 g; nitrobenzene: 4.5 mmol; benzyl alcohol: 45 mmol; mesitylene (solvent): 5 mL; Ar: 20 bar; T: 433 K; t: 3 h.
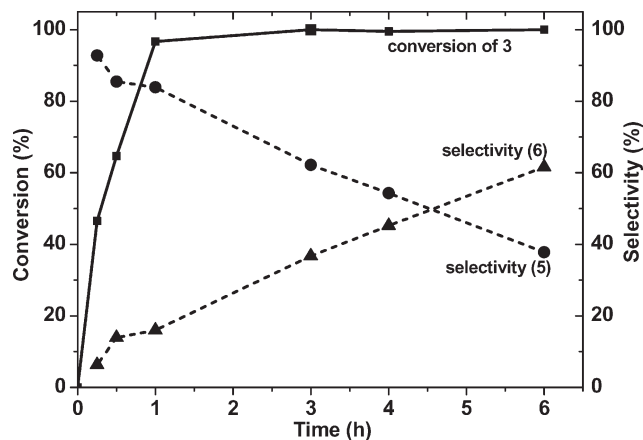
Fig. 3 Time-on-line profile of the nitrobenzene conversion and product selectivity for the tandem synthesis of **5** and **6** using the 1% RuPd/TiO$_2$ (M$_{Im}$) catalyst. Reaction conditions: catalyst: 0.1 g; nitrobenzene: 4.5 mmol; benzyl alcohol: 45 mmol; mesitylene (solvent): 5 mL; Ar: 20 bar; *T*: 433 K.

Table 1 Direct synthesis of *N*-benzylideneaniline (**5**) and *N*-benzylaniline (**6**) from benzyl alcohol (**1**) and nitrobenzene (**3**) using supported bimetallic catalysts[a]

Catalyst	Preparation method	Nitrobenzene conversion (%)	Product selectivity (%)	
			5	6
1% AuPd/TiO$_2$	S$_{Im}$	4	>99	—
1% Au–Pd/MgO	S$_{Im}$	3	>99	—
1% Au–Pd/TiO$_2$	M$_{Im}$	99	88	12
1% Au–Pd/MgO	M$_{Im}$	23	>99	—
1% Ru–Pd/TiO$_2$	M$_{Im}$	99	54	45
1% Ru–Pd/MgO	M$_{Im}$	26	>99	—
1% RuPd/C	M$_{Im}$	9	>99	—
1% RuPd/TiO$_2$[b]	M$_{Im}$	60	93	7
1% RuPd/TiO$_2$[c]	M$_{Im}$	32	97	3
1% RuPd/TiO$_2$[d]	M$_{Im}$	78	16	84

[a] Reaction conditions: catalysts: 0.1 g; nitrobenzene: 4.5 mmol; benzyl alcohol: 45 mmol; mesitylene (solvent): 5 mL; Ar: 20 bar; *T*: 433 K; *t*: 3 h. [b] Nitrobenzene: 4.5 mmol; benzyl alcohol: 22.5 mmol (benzyl alcohol *vs.* nitrobenzene = 5). [c] Nitrobenzene: 4.5 mmol; benzyl alcohol: 13.5 mmol (benzyl alcohol *vs.* nitrobenzene = 3). [d] Nitrobenzene: 4.5 mmol; benzyl alcohol: 4.5 mmol (benzyl alcohol *vs.* nitrobenzene = 1); reaction performed at 20 bar H$_2$.

of bimetallic catalysts have been reported that are superior for the oxidative dehydrogenation of benzyl alcohol compared to their monometallic analogues.[1,6,23] Based on this fact, and the sequence of reactions presented in Fig. 1, we hypothesize that the primary effect of the bimetallic catalyst is to enhance the rate of the initial dehydrogenation step, which has knock-on benefits for steps 2 and 3 (*i.e.* the production of *N*-benzylideneaniline and the secondary amine *N*-benzylaniline respectively).

Earlier, Sankar *et al.* have reported that, for the oxidative dehydrogenation of **1**, TiO$_2$-supported Au–Pd nano-alloys also catalyse an unwanted disproportionation reaction, resulting in the production of toluene and benzaldehyde, besides the desired dehydrogenation reaction to form benzaldehyde.[23] It was further reported that MgO-supported gold–palladium catalysts exclusively favour the dehydrogenation reaction by switching-off the disproportionation reaction.[23] A 1% AuPd/MgO (M$_{Im}$) catalyst was therefore also tested for the current hydrogen auto-transfer reaction, but was found to have a much lower activity (23% conversion) compared to the TiO$_2$-supported catalyst (99% conversion). An activated carbon-supported Ru–Pd catalyst also proved to be less active (9% conversion) (Table 1). In addition to the choice of support, the preparation method is also expected to strongly influence the activity, selectivity and stability of these supported bimetallic catalysts.[3,8] Prati *et al.* demonstrated the sol-immobilization (S$_{Im}$) technique as an effective way of preparing supported Au–Pd catalysts.[4] Hence, 1% Au–Pd/TiO$_2$ (S$_{Im}$) and 1% AuPd/MgO (S$_{Im}$) catalysts were also therefore tested in the hydrogen auto-transfer reaction for comparative purposes, but neither of these catalyst preparations proved to be very effective (Table 1) displaying only 4% and 3% conversion levels respectively. The catalytic results thus clearly show that the TiO$_2$-supported bimetallic catalysts prepared by the M$_{Im}$ route perform best in the direct synthesis of **5** and **6** from **1** and **3**. To further understand the role that the amount of **1**

has on the resultant activity, we performed reactions with different **1** to **3** molar ratios (*i.e.* **5** & **3**) using the best catalyst 1% RuPd/TiO$_2$ (M$_{Im}$) and the results are presented in Table 1. The results clearly indicate that the activity depends on the amount of benzyl alcohol present, or in other words, the extent of the dehydrogenation reaction. For the reaction with a **1** to **3** molar ratio of **5**, the molar conversion of **3** is 60% with a selectivity of 93% to product **5**. For the corresponding reaction performed with a molar ratio of **3**, the conversion is found to be 32% with 97% selectivity to product **5**. It is important to note that for all the other standard reactions reported in this article a molar ratio of 10 was used. Another approach to synthesize substituted amines is the reductive alkylation of nitrobenzene using benzyl alcohol (equimolar) as the alkylating agent under H$_2$ atmosphere. To test our bimetallic 1% RuPd/TiO$_2$ (M$_{Im}$) catalyst for this reductive alkylation reaction, we used an equimolar mixture of **1** & **3** under 20 bar of H$_2$. After 3 h of reaction, a 78% molar conversion of **3** was achieved with an 84% selectivity to product **6**. This result clearly indicates that this bimetallic catalyst is effective for the reductive alkylation reaction as well. Further optimization studies are currently in progress for this reaction.

The heterogeneous nature of the most active catalyst (1% Ru–Pd/TiO$_2$ (M$_{Im}$)) was demonstrated by three methods; namely (a) hot filtration, (b) ICP-MS analysis of the reaction mixture for metal content and (c) reusability of the recovered catalyst. These catalytic tests were performed in a 50 mL Radley's glass reactor held at 413 K and a pressure of 1 bar of He. In the hot filtration method, the catalyst was filtered off after 30 min (8% conversion) and the reaction mixture was allowed to react for a further 150 min under standard

This journal is © The Royal Society of Chemistry 2016

Catal. Sci. Technol., 2016, **6**, 5473–5482 | **5477**

reaction conditions. No increase in conversion (9%) and selectivity was seen after filtration (Fig. 4a). The reaction without catalyst removal had a conversion of 23% over the same time-period. ICP-MS measurements showed the filtered reaction mixture to contain negligible amounts of Ru and Pd (1.5% for Ru and 0.6% for Pd of the original amounts used in the reaction). Furthermore, the catalyst could be re-used three times without any loss in activity (8–9%). Interestingly however, the selectivity to **6** increased progressively from 27% for the fresh catalyst to 40% for the three-times used catalyst at the expense of **5** for the spent catalysts (Fig. 4b).

To characterize the composition and nanostructure of these highly active bimetallic M$_{Im}$ catalysts and to arrive at a structure/activity correlation, aberration corrected scanning transmission electron microscopy (AC-STEM) studies were carried out; the S$_{Im}$ catalysts have previously been extensively characterized and are not reported here.[6,7,23] Analysis of the

Fig. 4 (a) Confirming the heterogeneous nature of 1% Ru–Pd/TiO$_2$ (M$_{Im}$) catalyst by hot-filtration. For all the points shown the selectivity was found to be around 73% (imine) and 27% (amine). (b) Re-usability study of 1% Ru–Pd/TiO$_2$. Reaction conditions: nitrobenzene: 0.9 mmol; benzylalcohol: 8.6 mmol; mesitylene (solvent): 1 mL; 1% Ru–Pd/TiO$_2$: 0.020 g; temperature: 413 K; stirring speed: 500 rpm; time: 0.5 h; this reaction-set was performed in a moderate pressure glass reactor (Radleys®) fitted with a magnetic stirrer bar.

1% AuPd/TiO$_2$ M$_{Im}$ sample by high-angle annular dark-field (HAADF) – STEM imaging indicated that the mean size of the supported metal particles was ~1.5 nm (Fig. 5(a) and (b)). Even smaller sub-nm clusters were also apparent in this sample (Fig. S2(a)†) as were occasional very large μm-scale Au particles. X-ray energy dispersive spectroscopic (XEDS) analysis of individual nm-scale particles confirmed them to be Au–Pd alloys (Fig. 5(c) and (d)). A comparative HAADF-STEM study of the corresponding 1% RuPd/TiO$_2$ M$_{Im}$ sample shows that the mean size of the supported metal particles was slightly smaller at ~1.2 nm (Fig. 5(e) and (f)). Once again, many sub-nm clusters were apparent (Fig. S2(b)†), but in this case SEM analysis showed that the sample was devoid of any μm-scale metal particles. XEDS analysis confirmed that the nm-scale particles were indeed Ru–Pd alloys (Fig. 5(g) and (h)). To better understand how representative these structures are of the entirety of the catalyst sample, and to complement the STEM data, these catalysts were also characterised by X-ray absorption spectroscopy (XAS).[26]

The STEM observations of the presence of bimetallic species are confirmed by the XAFS data recorded at the Au L$_3$, Pd K and Ru K edges, respectively.[9] The Au and Pd XANES data for selected catalysts are given in Fig. 6, whilst the results from the analysis of the EXAFS data are given in Table 2 along with some example EXAFS spectra (including the results from the least squares fitting of the data) given in the ESI† (Fig. S3). The EXAFS data for the 1% Au–Pd/TiO$_2$ (M$_{Im}$) and 1% Ru–Pd/TiO$_2$ catalysts are reported in our recent article.[9] The Au L$_3$-edge data shown arise from a dipole-allowed transition of an initial 2p$_{3/2}$ electron to a 5d state and are therefore sensitive to changes in the electronic density of states (both initial and final).[27–29] When comparing the reference 1% Au/TiO$_2$ (M$_{Im}$) sample with that of the bimetallic 1% Au–Pd/TiO$_2$ samples (M$_{Im}$ and S$_{Im}$) we observe an enhancement of the feature at ~11 935 eV in the latter two samples which appears consistent with the formation of bimetallic species. This signal is proposed to arise as a result of charge transfer/electron donation from Au to the more electropositive Pd. Such charge transfer between Au and Pd leading to a slight positive charge build-up on Pd has previously been confirmed by XPS analysis of these materials.[9] This is accompanied by a 'blue shift' in the EXAFS oscillations, as well as a reduced oscillation frequency consistent with the formation of shorter Au–Pd bonds (as compared to the longer Au–Au bonds ~2.85 Å). That the particles are bimetallic can be seen immediately from the Fourier transform (FT) data. Two intense peaks in the FTs are observed as a consequence of a 'π phase flip' in the backscattering amplitude from 6 Å^{-1} for Au (or indeed for all elements where $Z > 78$) resulting in a splitting of the major contribution in the FT into a high and low R (distance) component. This occurs when two elements are present in equivalent amounts; often the splitting and intensity of the low r-space contribution becomes more intense with an increasing number of bimetallic bonds.[30–32] A similar effect is seen in the Pd K-edge FTs of the EXAFS data although a mismatch in the total coordination number
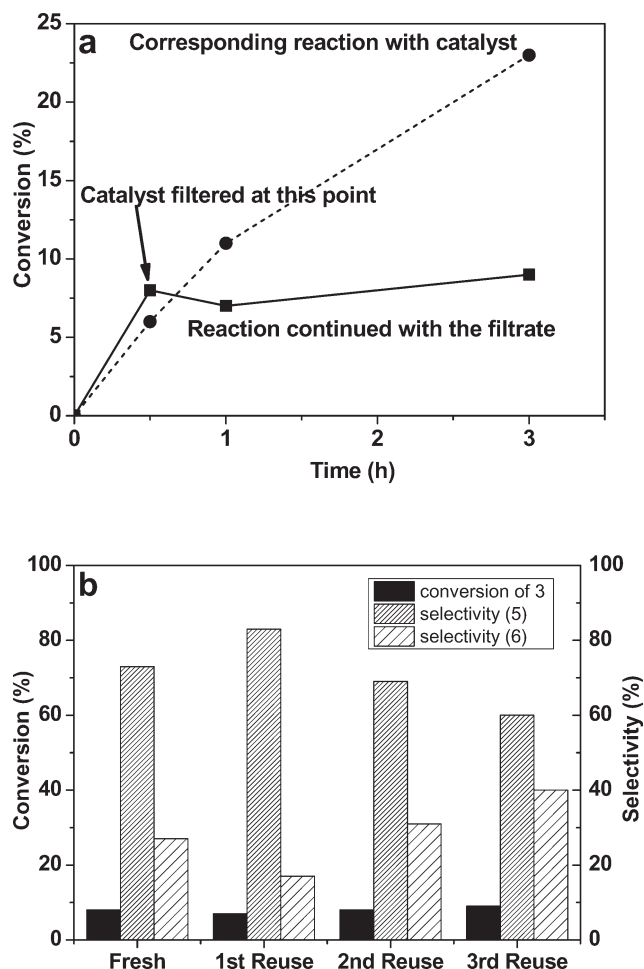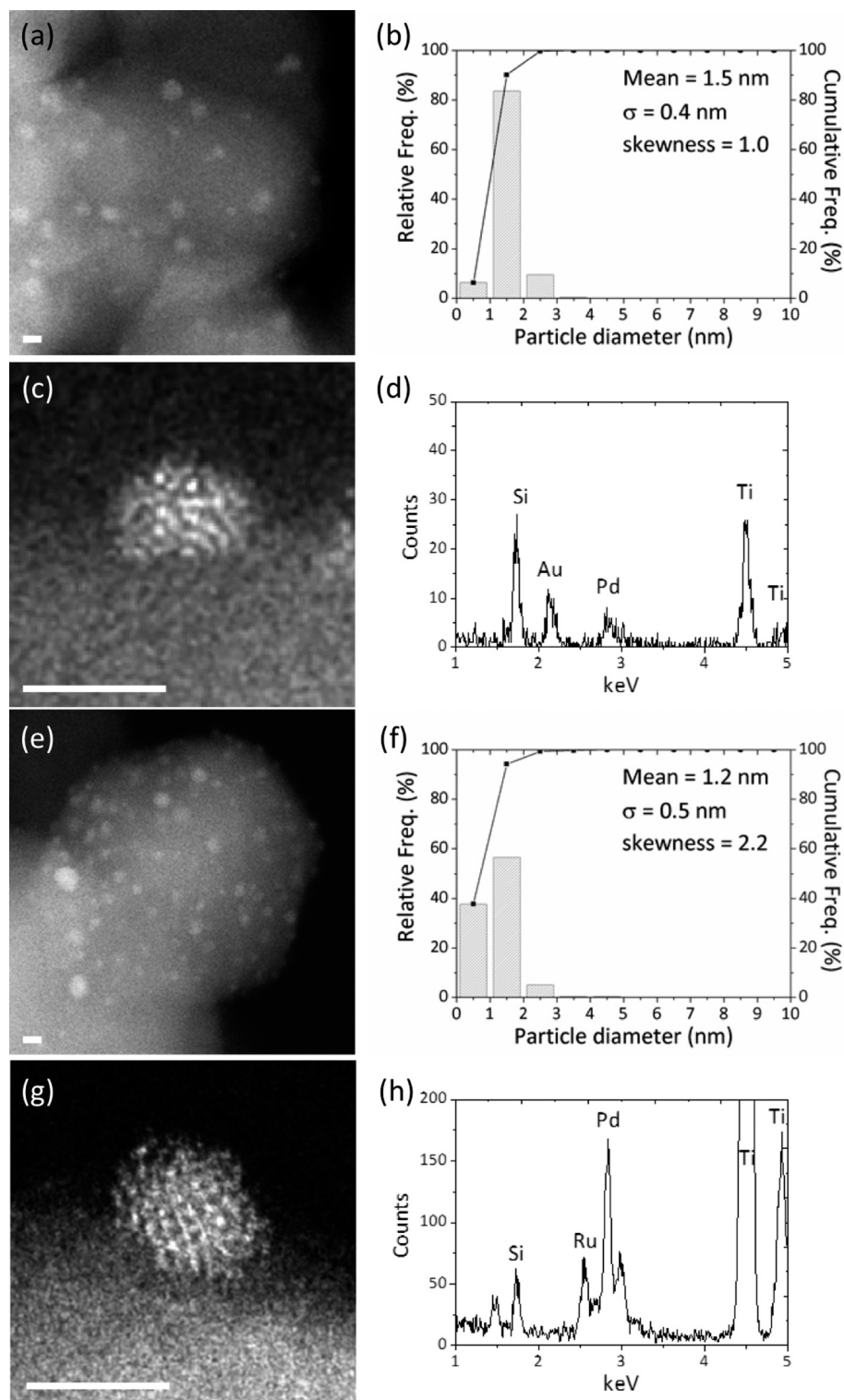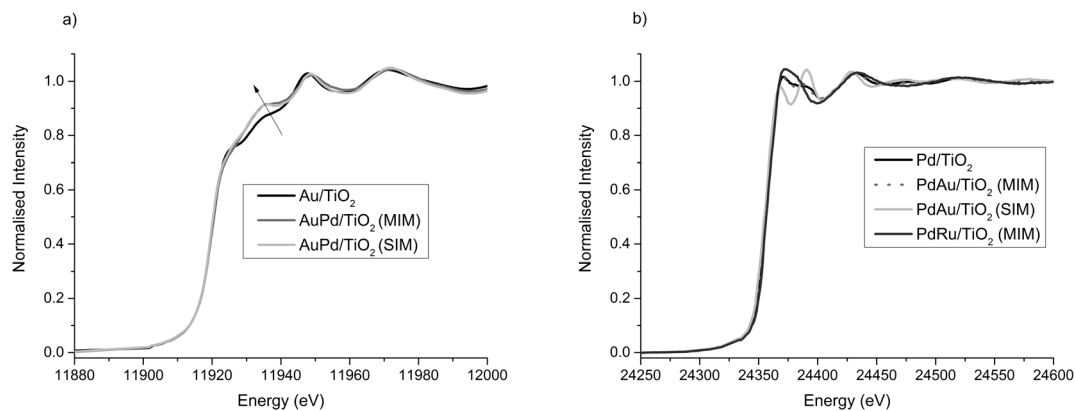
5478 | *Catal. Sci. Technol.*, 2016, **6**, 5473–5482

This journal is © The Royal Society of Chemistry 2016

Fig. 5 Representative STEM analyses of the 1% Au–Pd/TiO₂ (a, b, c & d) and 1% Ru–Pd/TiO₂ (e, f, g & h) samples prepared by the M_{Im} route. (a) HAADF image of 1% Au–Pd/TiO₂ showing typical particle sizes; (b) corresponding particle size distribution derived from measurement of over 500 particles; (c) HAADF image of an individual Au–Pd metal nanoparticle and (d) its corresponding XEDS spectrum confirming it is an Au–Pd alloy; (e) HAADF image showing typical particle sizes of 1% RuPd/TiO₂; (f) corresponding particle size distribution derived from measurement of over 500 particles; (g) HAADF image of an individual metal nanoparticle and (h) its corresponding XEDS spectrum confirming it is a Ru–Pd alloy. The scale bar in each image represents 2 nm.

This journal is © The Royal Society of Chemistry 2016

Catal. Sci. Technol., 2016, 6, 5473–5482 | 5479

Fig. 6 (a) Normalised Au L$_3$-edge XANES and (b) Pd K-edge XANES recorded for select monometallic and bimetallic catalysts. The arrow in (a) illustrates a greater transition intensity at *ca.* 11 935 eV for the bimetallic Au–Pd/TiO$_2$ samples due to electron transfer from Au to Pd.

Table 2 EXAFS parameters for the bimetallic catalysts determined from an analysis of the Au L$_3$, Pd K and Ru K-edges

Sample	Au–Au R (Å)	(N)	$2\sigma^2$ (Å^2)	Au–Pd (Å)	(N)	$2\sigma^2$ (Å^2)	Pd–Pd R (Å)	(N)	$2\sigma^2$ (Å^2)	Pd–Au R (Å)	N	$2\sigma^2$ (Å^2)	Ref.
1% Au–Pd/TiO$_2$ (S$_{Im}$)^a	2.8	7.8	0.017	2.78	4.1	0.014	2.75	4	0.014	2.78	3.9	0.016	Current Work^b
1% Au–Pd/TiO$_2$ (M$_{Im}$)^c	2.8	4.8	0.017	2.77	2.5	0.014	2.75	1	0.014	2.78	2.0	0.016	9
1% Au–Pd/MgO (M$_{Im}$)^d	2.79	8.0	0.017	2.73	3.3	0.014	2.72	3.5	0.014	2.75	2.9	0.016	Current Work
	Ru–O			Ru–Ru(Pd)			Pd–O			Pd–Pd(Ru)			
1% Ru–Pd/TiO$_2$ (M$_{Im}$)^e	2.0	3.0	0.011	2.69	2	0.023	2.0	2.7	0.009	2.72	1.8	0.019	9

$E_f \sim \pm15$ eV; R values for all data range from 28–38%. ^{a} A Pd–O contribution at 2.02 Å, $N = 0.3$, $2\sigma^2 = 0.013$ Å^2 is also present. ^{b} The EXAFS data and the associated Fourier transform data for this catalyst is presented in the ESI (Fig. S3). ^{c} A Pd–O contribution at 2.02 Å, $N = 1$, $2\sigma^2 = 0.0013$ Å^2 is also present. ^{d} A Pd–O contribution at 1.99 Å, $N = 1.3$, $2\sigma^2 = 0.013$ Å^2 is also present. ^{e} A Pd–O contribution at 1.99 Å, $N = 2$, $2\sigma^2 = 0.007$ Å^2 is also present. Afac values, 0.94 (Pd/Ru) and 0.98 Au. Debye–Waller factors were initially determined from the AuPd/TiO$_2$ S$_{Im}$ sample and not refined for the remaining AuPd samples.

from an analysis of the two edges has previously been shown to be due to the presence of large (~µm sized) Au particles in addition to bimetallic species and for the 1% Au–Pd/TiO$_2$ (M$_{Im}$) sample, atomically dispersed Pd species.[9] The Pd K-edge XANES data are less revealing regarding the extent of alloy formation, but are however, sensitive to the degree of Pd–O interactions. A greater rising absorption edge (lower density of states) is observed in the 1% Ru–Pd/TiO$_2$ (M$_{Im}$) sample which EXAFS data suggest contains the highest number of Pd–O neighbours (they are therefore the smallest particles and possess fewest number of metal–metal (M–M) bonds). It should be noted however that the similarity in X-ray scattering contrast between Pd and Ru precludes distinguishing between the two components of the bimetal in the EXAFS data although a first shell analysis assuming one M–M scatterer type could be performed on the basis that XEDS confirms the bimetallic nature of the sample.

The closeness in the coordination numbers of both species from an analysis of both edges supports the notion that the Pd and Ru exist in a similar environment (*i.e.* within intimately mixed bimetallic particles). Furthermore, the low coordination numbers obtained are consistent with the STEM analysis in that the particles are on average smaller than those seen for 1% Au–Pd/TiO$_2$ (M$_{Im}$). These observations from EXAFS and electron microscopy clearly indicate that

they are complimentary techniques for characterizing these supported bimetallic nano-alloys. From the above characterization data, it is evident that the bimetallic catalysts have a homogeneous random alloy structure.

Previously, we applied the most active bimetallic catalysts (1% AuPd/TiO$_2$ (M$_{Im}$), 1% RuPd/TiO$_2$) in a different reaction, namely the selective hydrogenation of levulinic acid, and reported in detail on their characterization.[9] Methods used included X-ray photoelectron spectroscopy (XPS), FF-IR of CO adsorption in addition to XAS and AC-STEM data of this material. FT-IR CO adsorption data clearly revealed that the electronic structure of both Au and Pd are modified by their close proximity to each other. This modification of the electronic structures of Au and Pd, where the Au atoms have a slight negative charge and the Pd atoms have slight positive charge, could be a contributing factor for the observed enhanced catalytic activity for the bimetallic Au–Pd catalyst. In the case of the Ru–Pd catalyst, it was very difficult to differentiate between Ru and Pd, however indirect evidence from all the characterisation techniques employed suggest that this material has a slightly smaller particle size compared to the Au–Pd catalyst. This stabilization effect, where the second metal stabilizes the smaller size of the first metal, could be the underlying reason for the enhanced catalytic activity of this latter material.

Conclusions

Supported gold–palladium and ruthenium–palladium bimetallic catalysts were prepared by a modified impregnation (M_{Im}) method. These catalysts were found to be exceptionally active for the direct synthesis of imines and secondary amines from nitroarenes and aromatic alcohols without using any hydrogen, sacrificial hydrogen donor and/or base using a hydrogen auto transfer strategy. This hydrogen auto transfer strategy is an alternative to those using H_2. Supported gold–palladium and ruthenium–palladium bimetallic catalysts were found to be several times more active (in terms of turnover number (TON)) than their monometallic counterparts. Bimetallic catalysts prepared by this M_{Im} method are also found to be more effective than their comparable catalyst formulations prepared by the more elaborate yet time-consuming, stabilizer-ligand assisted sol-immobilization (S_{Im}) method. TiO_2 was identified to be the best support for these bimetallic catalysts after comparing the catalytic activities of these bimetallics on a variety of support materials. AC-STEM and EXAFS characterization of the most active bimetallic catalysts prepared by M_{Im} method have revealed that these catalysts comprise of very small alloy particles with a narrow particle size distribution. They further suggest that the bimetallic particles have a homogeneous random alloy structure. In the case of Au–Pd system the charge transfer between Au and Pd, and in the case of Ru–Pd size stabilization effect have been correlated with the observed synergistic effect for the bimetallic catalysts. From a broader perspective, here we have demonstrated that the deliberate alloying of two metals in a highly controlled fashion can significantly enhance catalytic activity for a new class of hydrogen auto-transfer reactions as well as the more widely reported oxidation, reduction and hydrochlorination type reactions. This work implies that alloying using an appropriate combination of second metal choice and synthesis strategy could potentially increase the catalytic activity of many supported metal catalyst systems.

Acknowledgements

References

1 R. Ferrando, J. Jellinek and R. L. Johnston, *Chem. Rev.*, 2008, **108**, 845–910.

2 M. Sankar, N. Dimitratos, P. J. Miedziak, P. P. Wells, C. J. Kiely and G. J. Hutchings, *Chem. Soc. Rev.*, 2012, **41**, 8099–8139.

3 P. Paalanen, B. M. Weckhuysen and M. Sankar, *Catal. Sci. Technol.*, 2013, **2**, 2869–2880.

4 A. Villa, D. Wang, D. S. Su and L. Prati, *Catal. Sci. Technol.*, 2015, **5**, 55–68.

5 L. Prati and A. Villa, *Acc. Chem. Res.*, 2014, **47**, 855–863.

6 J. Pritchard, L. Kesavan, M. Piccinini, Q. He, R. Tiruvalam, N. Dimitratos, J. A. Lopez-Sanchez, A. F. Carley, J. K. Edwards, C. J. Kiely and G. J. Hutchings, *Langmuir*, 2010, **26**, 16568–16577.

7 R. C. Tiruvalam, J. C. Pritchard, N. Dimitratos, J. A. Lopez-Sanchez, J. K. Edwards, A. F. Carley, G. J. Hutchings and C. J. Kiely, *Faraday Discuss.*, 2011, **152**, 63–86.

8 M. Sankar, Q. He, M. Morad, J. Pritchard, S. J. Freakley, J. K. Edwards, S. H. Taylor, D. J. Morgan, A. F. Carley, D. W. Knight, C. J. Kiely and G. J. Hutchings, *ACS Nano*, 2012, **6**, 6600–6613.

9 W. Luo, M. Sankar, A. M. Beale, Q. He, C. J. Kiely, P. C. A. Bruijnincx and B. M. Weckhuysen, *Nat. Commun.*, 2015, **6**, 6540.

10 C. Gunanathan and D. Milstein, *Science*, 2013, **341**, 249.

11 T. Mallat and A. Baiker, *Chem. Rev.*, 2004, **104**, 3037–3058.

12 G. Guillena, D. J. Ramón and M. Yus, *Chem. Rev.*, 2009, **110**, 1611–1641.

13 A. J. A. Watson and J. M. J. Williams, *Science*, 2010, **329**, 635–636.

14 K.-I. Shimizu, *Catal. Sci. Technol.*, 2015, **5**, 1412–1427.

15 B. Chen, L. Wang and S. Gao, *ACS Catal.*, 2015, **5**, 5851–5876.

16 A. Zanardi, J. A. Mata and E. Peris, *Chem. – Eur. J.*, 2010, **16**, 10502–10506.

17 X. Cui, Y. Zhang, F. Shi and Y. Deng, *Chem. – Eur. J.*, 2011, **17**, 2587–2591.

18 C. Feng, Y. Liu, S. Peng, Q. Shuai, G. Deng and C.-J. Li, *Org. Lett.*, 2010, **12**, 4888–4891.

19 R. Cano, D. J. Ramón and M. Yus, *J. Org. Chem.*, 2011, **76**, 5547–5557.

20 L. Tang, H. Sun, Y. Li, Z. Zha and Z. Wang, *Green Chem.*, 2012, **14**, 3423–3428.

21 Q. Peng, Y. Zhang, F. Shi and Y. Deng, *Chem. Commun.*, 2011, **47**, 6476–6478.

22 C.-H. Tang, L. He, Y.-M. Liu, Y. Cao, H.-Y. He and K.-N. Fan, *Chem. – Eur. J.*, 2011, **17**, 7172–7177.

23 M. Sankar, E. Nowicka, R. Tiruvalam, Q. He, S. H. Taylor, C. J. Kiely, D. Bethell, D. W. Knight and G. J. Hutchings, *Chem. – Eur. J.*, 2011, **17**, 6524–6532.

24 S. Nikitenko, A. M. Beale, A. M. J. van der Eerden, S. D. M. Jacques, O. Leynaud, M. G. O'Brien, D. Detollenaere, R. Kaptein, B. M. Weckhuysen and W. Bras, *J. Synchrotron Radiat.*, 2008, **15**, 632–640.

25 B. Ravel and M. Newville, *J. Synchrotron Radiat.*, 2005, **12**, 537–541.

26 A. I. Frenkel, *Chem. Soc. Rev.*, 2012, **41**, 8163–8178.

27 R. J. Davis and M. Boudart, *J. Phys. Chem.*, 1994, **98**, 5471–5477.

This journal is © The Royal Society of Chemistry 2016

Catal. Sci. Technol., 2016, **6**, 5473–5482 | **5481**

28 S. N. Reifsnyder and H. H. Lamb, *J. Phys. Chem. B*, 1999, **103**, 321–329.

29 T. Balcha, J. R. Strobl, C. Fowler, P. Dash and R. W. J. Scott, *ACS Catal.*, 2011, **1**, 425–436.

30 A. M. Beale and B. M. Weckhuysen, *Phys. Chem. Chem. Phys.*, 2010, **12**, 5562–5574.

31 A. G. McKale, B. W. Veal, A. P. Paulikas, S. K. Chan and G. S. Knapp, *Phys. Rev. B: Condens. Matter Mater. Phys.*, 1988, **38**, 10919–10921.

32 J. M. Cowley, *Phys. Rev.*, 1965, **138**, A1384–A1389.